International Journal of Solids and Structures 47 (2010) 1306–1316

Contents lists available at ScienceDirect

International Journal of Solids and Structures

journal homepage: www.elsevier.com/locate/ijsolstr

Constitutive modeling of shape memory polymer based self-healing syntactic foam

We Xu [a], Guoqiang Li [a,b,*]

[a] Department of Mechanical Engineering, Louisiana State University, Baton Rouge, LA 70803, USA
[b] Department of Mechanical Engineering, Southern University, Baton Rouge, LA 70813, USA

ARTICLE INFO

Article history:
Received 21 October 2009
Received in revised form 14 January 2010
Available online 22 January 2010

Keywords:
SMP
Syntactic foam
Self-healing
Thermomechanics
Constitutive model
Stress strain recovery

ABSTRACT

In a previous study, it was found that the shape memory functionality of a shape memory polymer based syntactic foam can be utilized to self-seal impact damage repeatedly, efficiently, and almost autonomously [Li G., John M., 2008. A self-healing smart syntactic foam under multiple impacts. Comp. Sci. Technol. 68(15–16), 3337–3343]. The purpose of this study is to develop a thermodynamics based constitutive model to predict the thermomechanical behavior of the smart foam. First, based on DMA tests and FTIR tests, the foam is perceived as a three-phase composite with interfacial transition zone (interphase) coated microballoons dispersed in the shape memory polymer (SMP) matrix; for simplicity, it is assumed to be an equivalent two-phase composite by dispersing elastic microballoons into an equivalent SMP matrix. Second, the equivalent SMP matrix is phenomenologically assumed to consist of an active (rubbery) phase and a frozen (glassy) phase following Liu et al. [Liu, Y., Gall, K., Dunn, M.L., Greenberg, A.R., Diani J., 2006. Thermomechanics of shape memory polymers: uniaxial experiments and constitutive modeling. Int. J. Plasticity 22, 279–313]. The phase transition between these two phases is through the change of the volume fraction of each phase and it captures the thermomechanical behavior of the foam. The time rate effect is also considered by using rheological models. With some parameters determined by additional experimental testing, the prediction by this model is in good agreement with the 1D test result found in the literature. Parametric studies are also conducted using the constitutive model, which provide guidance for future design of this novel self-healing syntactic foam and a class of light-weight composite sandwich structures.

1. Introduction

Syntactic foams, a class of composites made of a polymeric matrix filled with hollow particulate inclusions, renowned for its low density and high specific mechanical properties, are currently enjoying continuous growth in various civilian and military sectors. Their typical applications range from buoyancy materials for submarines to cushion materials for packing (Anderson et al., 1970). The versatility and applicability of such composites attracts interest from numerous researchers and thus propels many characteristic-improvement studies such as functionally grading syntactic foams (El-Hadek and Tippur, 2003; Gupta, 2007) and toughened syntactic foams (Li and Nji, 2007; Li and John, 2008; Nji and Li, 2008), as well as analytical modeling of constitutive behavior (Rizzi et al., 2000; Song et al., 2004). Because of the improved mechanical/functional properties, a tendency is found that syntactic foams are being increasingly used in high performance load-bearing structures such as foam cored sandwich, grid stiffened foam cored sandwich, etc. (Li and Muthyala, 2008; Li and Chakka, 2010). However, like other composite structures, foam cored or hybrid foam cored sandwich structures are still vulnerable to impact damage. Self-healing or self-mending of structural damage is desired.

One of the grand challenges facing self-healing community is how to heal macroscopic or structural scale damage such as impact damage autonomously, repeatedly, efficiently, and at molecular-length scale. For the existing self-healing schemes such as microcapsules (Blaiszik et al., 2008), hollow fibers (Pang and Bond, 2005), microvascular networks (Toohey et al., 2007), ionomers (Varley and van der Zwaag, 2008), thermally reversible covalent bonds (Liu and Chen, 2007), thermal plastic particle additives (Zako and Takano, 1999), etc., they are very effective in self-healing micro-length scale damages. However, they face tremendous challenges when they are used to heal large, millimeter-scale, structural damage. The reason for this is that structural damage needs a sufficient amount of healing agent to fill in the crack. However, incorporation of a large amount of healing agent such as thermoplastic particles will significantly alter the physical/mechanical properties of the host structure. Also, large capsules or thick hollow fibers themselves may become potential defects when the encased healing agent is released. Although ionomer has been proved to

* Corresponding author. Address: Department of Mechanical Engineering, Louisiana State University, Baton Rouge, LA 70803, USA. Tel.: +1 225 578 5302; fax: +1 225 578 5924.
E-mail address: guoli@me.lsu.edu (G. Li).

0020-7683/$ - see front matter © 2010 Elsevier Ltd. All rights reserved.
doi:10.1016/j.ijsolstr.2010.01.015

self-heal ballistic impact damage (Varley and van der Zwaag, 2008), it inherently utilized the rebound of the broken ionomers. Without the elastic rebound, the broken pieces cannot be brought into contact and ionomer cannot self-heal itself, either.

Because of this, we propose that a sequential two-step scheme be used by mimicking the biological healing process such as human skin: seal then heal (STH). In STH, the structural scale crack will be first sealed or closed by a certain mechanism before the existing self-healing mechanisms such as microcapsule or thermoplastic particles take effect. Shape memory polymer (SMP), due to its autonomous, conformational entropy driven shape recovery properties, can be utilized to achieve the self-sealing purposes. In a previous study, it has been proved that the confined shape recovery of a shape memory polymer based syntactic foam is able to seal impact damage repeatedly, efficiently, and almost autonomously (Li and John, 2008). It is believed that if the existing micro-length scale repairing scheme such as microcapsules or thermoplastic particles are incorporated into the SMP matrix, a two-step (seal then heal) self-healing scheme could be achieved and the healing would be achieved repeatedly, efficiently, almost autonomously, and at molecular-length scale.

The objective of this study is to develop a constitutive model to predict the thermomechanical behavior of this novel foam so that it can be optimized for advanced mechanical and self-healing properties. While considerable experimental investigations of SMP have been reported in the literature (Tobushi et al., 1996, 1998; Liu et al., 2004), fundamental knowledge of the constitutive relationship for the thermomechanical properties of SMP remains an emerging topic. Although earlier efforts (Tobushi et al., 1997; Bhattacharyya and Tobushi, 2000) using rheological models were able to describe the characteristic thermomechanical behavior of SMP, the loss of the strain storage and release mechanisms usually led to limited prediction accuracy. Later, other approaches such as mesoscale model (Kafka, 2001, 2008) and molecular dynamic simulation (Diani and Gall, 2007) were further developed to understand the mechanisms at a rather detailed level. Recently, various phenomenological approaches (Morshedian et al., 2005; Gall et al., 2005; Liu et al., 2006; Yakacki et al., 2007; Qi et al., 2008; Chen and Lagoudas, 2008a,b; Nguyen et al., 2008) have been developed to interpret the thermomechanical behavior of SMP from a macroscopic viewpoint. With different underlying hypotheses, these approaches can be roughly divided into two categories. Liu et al. (2006) adopted a first-order phase transition concept and modeled the SMP as a continuum mixture of a frozen and an active phase. The frozen phase and active phase represented two different configurations for temperature below and above the glass transition temperature (θ_g). And a term of stored strain (ε_s) was introduced to identify the strain storage and release mechanisms. The parameters of their model can be easily determined by simple macroscopic testing and the simulation reasonably captures the essential shape memory responses. However, the model simplified the SMP as a special elastic problem hence did not consider the time-dependence of the material. And a notable controversy was that it did not represent the physical processes of the glass transition and thus resulted in nonphysical parameters, such as volume fraction of the frozen phase. To address such issues, Nguyen et al. (2008) investigated the shape memory behavior through a structural and stress relaxation mechanism. They proposed that the shape memory phenomena of SMP were primarily motivated by the dramatic change of molecular chain mobility induced by the glass transition. The chain mobility underpins the ability of the chain segments to rearrange locally to bring the macromolecular structure and stress response to equilibrium, suggesting that the structure relaxes instantaneously to the equilibrium state at high temperature but responds sluggishly during cooling. Such behavior macroscopically freezes the structure at a low temperature in a non-equilibrium configuration thus allows the material to store a temporary shape. Reheating restores the mobility and allows the shape recovery. The important feature of this approach is that it reasonably and physically interprets the underlying mechanism for shape memory effects and the time-dependence behavior of the shape memory can be reproduced. However, the utilization of the model requires the incorporation of many other sophisticated models, which not only complicates the entire constitutive model but also requires some additional fundamental assumptions. It is noticed that some of these hypotheses such as the free energy activation parameter in the Adams-Gibbs model which was considered to be invariant to the temperature and pressure are still debatable (Tüdős and David, 1996; Andreozzi et al., 2004).

Since our focus is on establishing a theoretical framework that captures the shape memory effects of the self-healing foam, the simplified two-phase concept (frozen phase and active phase) of Liu et al. (2006) is employed to formulate the equivalent SMP matrix. To be more realistic, we further provide the model with predictive ability for the time-dependent behavior of the foam.

The current paper will be presented in the following sections. First, experimental evidence will be provided using FTIR and DMA to deduce the three-phase microstructure of the syntactic foam (interfacial transition zone coated glass microballoons dispersed in the SMP matrix). For simplicity, the three-phase syntactic foam will be treated as an equivalent two-phase composite material with glass microballoons dispersed in an equivalent SMP matrix. As did by Liu et al. (2006), the equivalent SMP will be further subdivided into two phases (frozen phase and active phase), and the 3D constitutive model will be developed. In order to consider the viscoelastic and viscoplastic behavior, the time rate effect will be considered by using rheological models. The constitutive model will then be examined against the second thermodynamic law for compatibility. With additional tests such as coefficient of thermal expansion test, the model prediction will be compared with a 1D stress-controlled programming and 1D strain controlled stress recovery and free-strain recovery test results of an SMP based syntactic foam by Li and Nettles (2009). Finally, parametric studies will be conducted to provide some guidance for future design of this novel syntactic foam.

2. Experimental investigation

As shown in the SEM picture in Fig. 1, the SMP based syntactic foam is formed by dispersing glass microballons in the SMP matrix. However, since the fabrication of the syntactic foam involves a series of chemical reactions, the interaction between the microballoons and the polymer matrix may not be just the physical contact. Berriot et al. (2003) discovered that a long-ranged gradient of the matrix glass transition temperature existed in the vicinity of the silica inclusions, suggesting that an interfacial transition zone (ITZ) may be present. In order to validate the possible chemical interactions and further facilitate formulation, several typical experiments are conducted on the foam.

2.1. Raw materials and curing

The syntactic foam consists of hollow glass microballoons dispersed in a shape memory polymer matrix. The polymer is a styrene based thermoset SMP resin system ($\theta_g = 62\ ^\circ C$) by CRG Industries under the name *Veriflex*. The glass microballoons were from Potters Industries (Q-CEL 6014: 85 μm average outer diameter, effective density of 0.14 g/cm^3, and 0.8 μm wall thickness). These raw materials have been used previously for the smart syntactic foam (Li and Nettles, 2009).

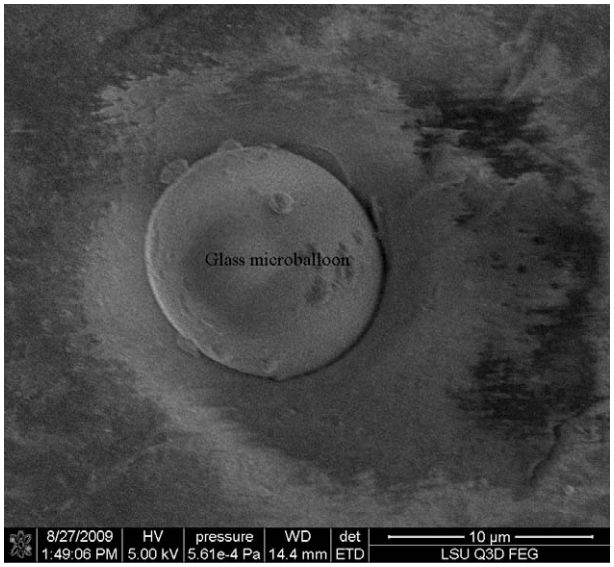

Fig. 1. SEM image of a SMP based syntactic foam sample.

The SMP based syntactic foam was fabricated by dispersing 40% by volume of glass microspheres into the SMP resin. The microspheres were added incrementally, with several minutes of mechanical blending between additions. A hardening agent was then added and the solution mixed for 10 min. The composite was poured into a 229 × 229 × 12.7 mm steel mold and placed in a vacuum chamber at 40 kPa for 20 min in order to remove any air bubbles entrapped in the matrix. The curing cycle was 79 °C for 24 h, 107 °C for 3 h, and 121 °C for 9 h. After curing, the foam panel was de-molded and was machined into different geometry for various testing. This foam is the same as the one used by Li and Nettles (2009).

2.2. Dynamic mechanical analysis

The dynamic mechanical analysis (DMA) test was conducted on a DMA 2980 tester from TA instruments. A rectangular bar with dimensions of 17.5 mm × 11.9 mm × 1.20 mm was placed into a DMA single cantilever clamping fixture. A small dynamic load at 1 Hz was applied to the platen and the temperature was ramped from room temperature to 120 °C at a rate of 3 °C/min. The amplitude was set to 15 μm. The glass transition temperature θ_g was determined from the storage modulus curve as suggested by ASTM E 1640-04.

2.3. Fourier transform infrared (FTIR) spectroscopy analysis

Fourier transform infrared (FTIR) spectra of both the pure polymer and the foam sample were recorded on a Bruker Tensor 27 single beam instrument at 16 scans with a nominal resolution of 4 cm^{-1}. Absorption spectra were saved from 4000 to 700 cm^{-1}.

2.4. Coefficient of thermal expansion measurement

The coefficient of thermal expansion (CTE) was measured by using the Vishay BLH SR-4 general-purpose strain gages and a Yokagawa DC100 data acquisition system. The test procedure followed the Tech note TN-513 (Vishay Micro Measurement, 2007). The reference material was Aluminum alloy. Both the test and reference sample dimensions were 30 mm × 12 mm × 5 mm. The temperature was ramped from room temperature to 90 °C at an average heating rate of 1 °C/min and then naturally cooled down to room temperature.

3. Modeling

3.1. Facts and assumptions

According to the DMA results (Fig. 2), it is found that the glass transition temperature of the foam has been shifted up as compared to that of the pure SMP. This suggests that some chemical reaction may have occurred at the glass microballoon/SMP interface. The mobility of the SMP polymer in the vicinity of the interface has been confined and reduced, leading to an increase in glass transition temperature. This has been further evidenced by the FTIR test results. Fig. 3 indicates that the intensity ratio of the two peaks around 1746 and 1724 cm^{-1} (the peaks marked in red) changed after the incorporation of the microballoons, which implies that some hydrogen bonds may have been formed and chemical reaction at the interface probably occurred.

Of course, in order to make sure that the change is due to chemical reaction but not due to the physical presence of the microballoons, a control test, i.e., incorporating microballoons with defunctionalized surface coatings to prevent chemical activity, would be helpful. Although there still exists uncertainty about the origin of the change of material properties after the incorporation of glass microballoons, it can be concluded that an interfacial transition zone (ITZ) probably exists in the syntactic foam and the foam can be perceived as a three-phase composite with ITZ coated microballoons dispersed in the SMP matrix.

As mentioned previously, it is known that the gradient of the glass transition temperature of the polymer can be very large across the thin layer of interfacial transition zone (Berriot et al., 2003). Because the current techniques cannot determine the detailed profile of the glass transition temperature in the ITZ layer, it is convenient to treat the ITZ and the pure SMP matrix as an equivalent SMP medium.

Hence, several assumptions have been made in this study:

(1) The foam system is treated as a two-phase composite with glass microballoons dispersed in an equivalent SMP matrix (Fig. 5), and is considered to be macroscopically homogeneous, meaning that the stress field is uniform everywhere. Also the temperature is assumed uniform over the entire body.
(2) The equivalent SMP matrix is considered as a two-phase mixture (Liu et al., 2006): the active phase and the frozen phase. The frozen phase is responsible for the strain storage. When the frozen phase passes through a frozen material

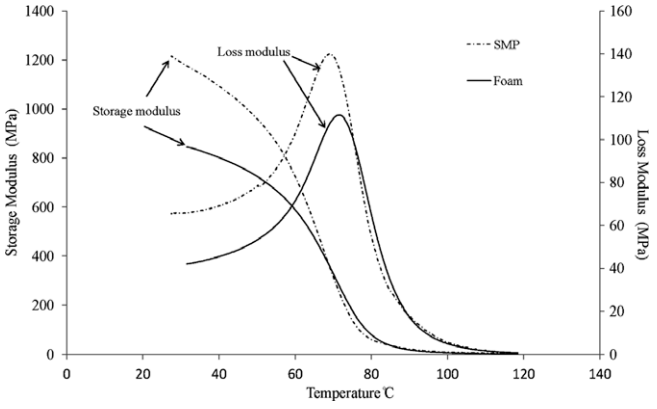

Fig. 2. DMA results for the pure SMP and syntactic foam.

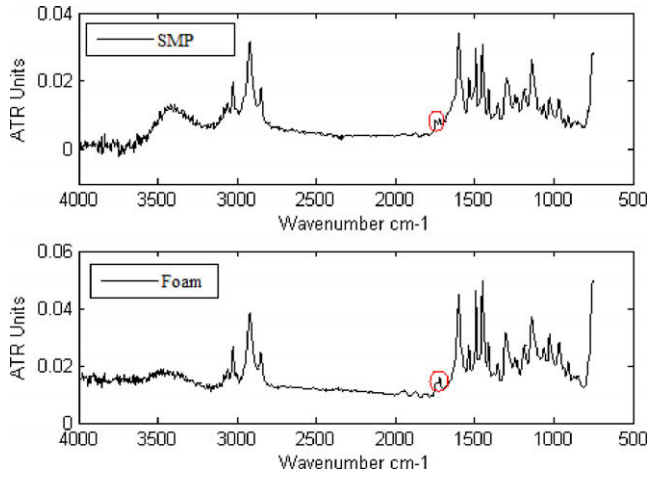

Fig. 3. FTIR spectra of the pure SMP and syntactic foam.

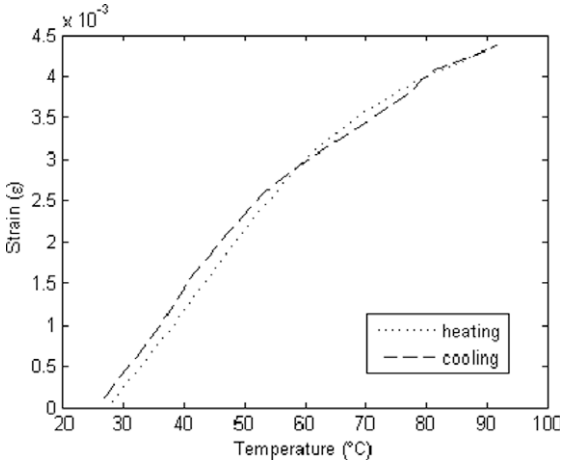

Fig. 4. Thermal expansion strain measured using strain gages.

point again during subsequent heating, the stored deformation at such point is fully recovered and the frozen phase becomes the active phase.

3.2. Constitutive model

Let Ω_0 denote the initial reference configuration of an undeformed and unheated continuum body, while Ω denotes the spatial configuration of the deformed body which may also experience the temperature change. If the nonlinear mapping of a material point $\boldsymbol{X} \in \Omega_0$ to Ω can be defined as a function of location, temperature and time: $\boldsymbol{x}=\boldsymbol{x}(\boldsymbol{X}, \theta(t),t)$, the tangent of the deformation map defines the deformation gradient $\mathbf{F} = \frac{\partial \boldsymbol{x}}{\partial \boldsymbol{X}}$. To separate the thermal and mechanical deformation we introduce the multiplicative decomposition of the thermomechanical deformation gradient into thermal and mechanical components (Lu and Pister, 1975; Lion, 1997):

$$\mathbf{F} = \mathbf{F}_M \mathbf{F}_\theta, \tag{1}$$

As shown in Fig. 6, the thermal component $\mathbf{F}_\theta$ is a mapping from Ω_0 to an intermediate heated configuration Ω_θ.

The mechanical component $\mathbf{F}_M$ can be further split multiplicatively into reversible and irreversible components (Kröner, 1960; Lee, 1969):

$$\mathbf{F}_M = \mathbf{F}_r \mathbf{F}_{ir} \tag{2}$$

where $\mathbf{F_r}$ is the reversible component and $\mathbf{F_{ir}}$ is the irreversible component.

As discussed previously, the foam can be first treated as a composite material which has glass microballoons as the dispersed phase and equivalent SMP as the matrix or continuous phase. With the initial assumptions of spatially uniform temperature and stress field and with the help of the average scheme, the reversible deformation can be expressed as:

$$\mathbf{F}_r = f_g \mathbf{F}_g + f_p \mathbf{F}_p \tag{3}$$

where f denotes the volume fraction, subscripts g and p denote glass microballoon and the equivalent SMP matrix, respectively $f_g + f_p = 1$.

The equivalent SMP matrix, as elaborated earlier, is considered to be composed of two phases: the active phase and the frozen phase. An implication of Assumption 2 in Section 3.1 is that the deformation gradient at a material point is in general discontinuous when heating from the frozen phase to the active phase. And whenever a material point is in the active phase, it does not "remember" its states in the previous frozen state (Chen and Lagoudas, 2008a).

Therefore, the deformation gradient at a material point in the equivalent SMP matrix can be described as:

$$\mathbf{F}_p(\boldsymbol{X}, t) = \begin{cases} \mathbf{F}_a(\boldsymbol{\sigma}(\boldsymbol{X}, t), \theta(\boldsymbol{X}, t), t), & \text{if } \boldsymbol{X} \in \Omega_a \\ \mathbf{F}_f(\boldsymbol{\sigma}(\boldsymbol{X}, t)), \theta(\boldsymbol{X}, t), t))\tilde{\mathbf{F}}, & \text{if } \boldsymbol{X} \in \Omega_f \end{cases} \tag{4}$$

where the subscripts a and f denote the active phase and the frozen phase, respectively. $\boldsymbol{\sigma}$ is the stress tensor. $\tilde{\mathbf{F}}$, the deformation gradient from the original reference configuration to the frozen reference configuration, represents the redistribution of deformation due to the history dependence of the frozen phase. Ω_a and Ω_f denote the active region and the frozen region, respectively. Their relationship with the equivalent SMP matrix domain Ω_p can be expressed as:

$$\Omega_a \cup \Omega_f = \Omega_p, \tag{5}$$

We then apply the average to the deformation gradient of the equivalent matrix over Ω_p,

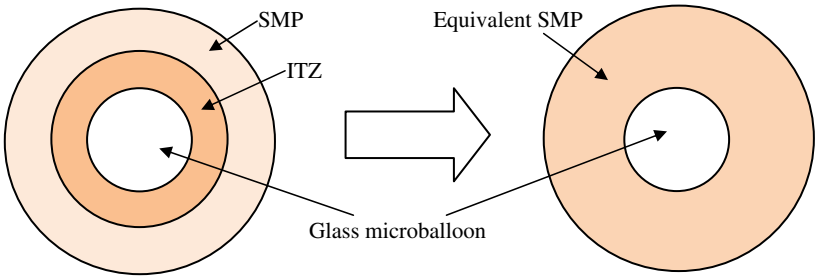

Fig. 5. A general model scheme.

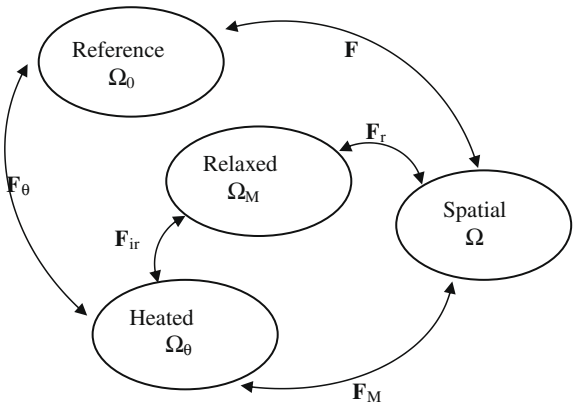

Fig. 6. An analogous decomposition scheme for the deformation gradient.

$$\mathbf{F}_p(\boldsymbol{X},t) = (1-\phi)\mathbf{F}_a(\boldsymbol{\sigma},\theta,t) + \int_{t_0}^{t} \mathbf{F}_f(\boldsymbol{\sigma},\theta,t)\tilde{\mathbf{F}}(\tau)\phi'(\tilde{\theta}(\tau))d\tau \tag{6}$$

here $\tilde{\theta}(\tau)$ physically represents the maximum temperature the material experiences immediately before it is frozen. $\phi(\theta) = \Omega_f/\Omega_p$ is the frozen phase volume fraction. If we consider that the growth of the frozen region only depends on the temperature and the equivalent SMP can be assumed to be statistically homogeneous, the statement that the frozen region growth during cooling can be expressed as:

$$\phi(\theta_2) > \phi(\theta_1) \quad \text{if} \quad \theta_1 > \theta_2, \tag{7}$$

and when θ_0 is well above θ_g, $\phi(\theta_0) = 0$,

Finally, the total deformation gradient of the foam body yields:

$$\mathbf{F} = \left(f_g\mathbf{F}_g + f_p\left((1-\phi)\mathbf{F}_a(\boldsymbol{\sigma},\theta,t) + \int_0^t \mathbf{F}_f(\boldsymbol{\sigma},\theta,t)\tilde{\mathbf{F}}\phi'(\tau)d\tau\right)\right)\mathbf{F}_{\mathbf{ir}}\mathbf{F}_\theta, \tag{8}$$

In the classical theory of mechanics, the Cauchy strain ε is related to the deformation gradient through

$$\boldsymbol{\varepsilon} = \frac{1}{2}(\mathbf{F} + \mathbf{F}^{\mathbf{T}}) - \mathbf{I}, \tag{9}$$

and also

$$\mathbf{F} = \mathbf{I} + \frac{\partial \mathbf{u}}{\partial X}, \tag{10}$$

where **u** is the displacement tensor.

If we only consider the linear deformation, we have

$$\mathbf{F}_1\mathbf{F}_2 = \mathbf{F}_1 + \mathbf{F}_2 - \mathbf{I}, \tag{11}$$

Then the strain field in the SMP based syntactic foam material can be obtained:

$$\boldsymbol{\varepsilon} = (1-f_p)\boldsymbol{\varepsilon}_g + f_p((1-\phi)\boldsymbol{\varepsilon}_a + \phi\boldsymbol{\varepsilon}_f + \boldsymbol{\varepsilon}_s) + \boldsymbol{\varepsilon}_{ir} + \boldsymbol{\varepsilon}_\theta, \tag{12}$$

where $\boldsymbol{\varepsilon}_s = \int_{t_0}^{t} \tilde{\boldsymbol{\varepsilon}}(\tau)\phi'(\tau)d\tau$ is the stored strain. In the paper by Liu et al. (2006), this terminology is considered as an internal variable depending on temperature only. Thus, it can be obtained from the cooling process where it is defined as:

$$\boldsymbol{\varepsilon}_s = \int_{t_0}^{t} \boldsymbol{\varepsilon}_a(\tau)\phi'(\tau)d\tau, \tag{13}$$

meaning that the stored strain comes from the entropic strain in the active phase.

The other terms in Eq. (12) are analyzed as follows:

3.2.1. Glass microballoons

The glass microballoons are considered to be fully linear elastic. Then the Cauchy strain can be defined as:

$$\boldsymbol{\varepsilon}_g = \mathbf{S}_g\boldsymbol{\sigma}. \tag{14}$$

where **S** is the compliance tensor.

3.2.2. Active phase

There are quite a few sophisticated models trying to capture the behavior of the polymers at temperature above θ_g (Boyce and Arruda, 1993; Kontou, 2005; Khan et al., 2006). The combination of the Maxwell and Kelvin elements in series is often used to describe in simple terms the viscoelastic deformation of polymers (Sperling, 2006). As demonstrated previously, the overall deformation has been split into the reversible and the irreversible component. It is therefore possible to capture the reversible deformation behavior of the active phase using a linear viscoelastic rheological model shown in Fig. 7(a). The Cauchy strain tensor can then be defined as:

$$\boldsymbol{\varepsilon}_a = \boldsymbol{\varepsilon}_a^e + \boldsymbol{\varepsilon}_a^v, \tag{15}$$

and the Cauchy stress tensor is:

$$\boldsymbol{\sigma} = \mathbf{C}_a^e\boldsymbol{\varepsilon}_a^e = \mathbf{C}_a^r\boldsymbol{\varepsilon}_a^v + \gamma_a\dot{\boldsymbol{\varepsilon}}_a^v, \tag{16}$$

where superscripts e, v, and r denote the elastic, the viscous and the rubbery parts. **C** is the stiffness tensor and $\boldsymbol{\gamma}$ is the viscosity tensor.

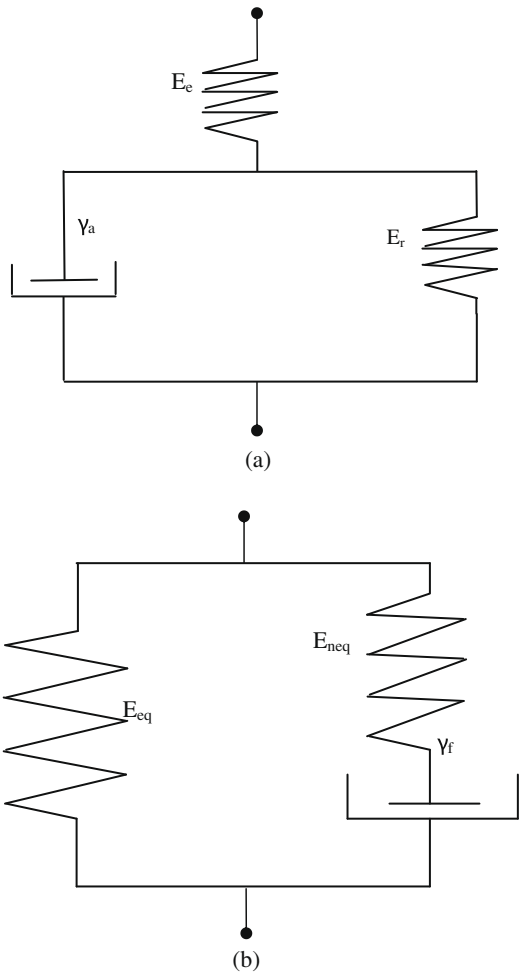

Fig. 7. Linear rheological representation of (a) the active phase and (b) the frozen phase.

3.2.3. Frozen phase

The viscoplastic behavior of a polymer at the temperature below θ_g can be captured by decomposing the stress response into an equilibrium time-independent behavior and a non-equilibrium time-dependent behavior (Qi et al., 2008). Fig. 7(b) shows the rheological scheme. Thus, the total Cauchy stress tensor is:

$$\boldsymbol{\sigma} = \boldsymbol{\sigma}_{\mathrm{f}}^{\mathrm{eq}} + \boldsymbol{\sigma}_{\mathrm{f}}^{\mathrm{neq}} = \mathbf{C}_{\mathrm{f}}^{\mathrm{r}}\boldsymbol{\varepsilon}_{\mathrm{f}}^{\mathrm{eq}} + \boldsymbol{\sigma}_{\mathrm{f}}^{\mathrm{neq}} \tag{17}$$

The non-equilibrium component is described as:

$$\dot{\boldsymbol{\varepsilon}}_{\mathrm{f}}^{\mathrm{eq}} = (\mathbf{S}_{\mathrm{f}}^{\mathrm{e}}\dot{\boldsymbol{\sigma}}_{\mathrm{f}}^{\mathrm{neq}} + \boldsymbol{\sigma}_{\mathrm{f}}^{\mathrm{neq}}), \tag{18}$$

here superscripts eq and neq denote the equilibrium and the non-equilibrium components. Also it should be noted that $\boldsymbol{\varepsilon}_{\mathrm{f}}^{\mathrm{eq}} = \boldsymbol{\varepsilon}_{\mathrm{f}}$.

To further consider the post-yielding strain softening behavior, a bi-viscosity model that the original viscosity decreases to a value after yielding can be assumed, although there exist other more complicated models such as the activation volume evolution with respect to deformation through a probability density function assumption proposed by Kontou (2005), which captures such feature as well.

3.2.4. Evolution rules for the frozen fraction ϕ

In a thermomechanical cycle, the change of the frozen fraction ϕ controls the strain storage and release. Since we only consider the equilibrium phase separation condition, the frozen fraction function is considered to be dependent on temperature only. A phenomenological function of the frozen fraction has been introduced (Qi et al., 2008):

$$\phi = 1 - \frac{1}{1 + \exp(-(\theta - \theta_{ref})/A)}, \tag{19}$$

where θ_{ref} is a reference temperature at which $\phi = \frac{1}{2}$. Thus, it is reasonable to choose θ_{g} as θ_{ref} if we consider the definition of the glass transition temperature (Chen and Lagoudas, 2008a). A is a parameter determining the width of the phase transition zone. It can be obtained from curve-fitting of the experimental results. In a uniaxial free recovery test, ϕ is in fact the ratio of scalar $\varepsilon^{*}/\varepsilon_{\mathrm{pre}}$ (Liu et al., 2006), where in our case ε^{*} is the modified recovery strain by subtracting the thermal strain and irreversible strain from the recovery strain. And $\varepsilon_{\mathrm{pre}}$ denotes the pre-deformation strain, which is obtained by subtracting the thermal strain and irreversible strain from the fixed-strain.

3.2.5. Thermal strain

The thermal strain can be expressed in terms of thermal expansion coefficient α.

If the isotropic thermomechanical response is further assumed, the thermal strain is:

$$\boldsymbol{\varepsilon}_{\theta} = \int_{\theta_0}^{\theta} \alpha \cdot \mathbf{I} d\theta \tag{20}$$

In order not to lose generality (Fig. 4), α is considered as a function of temperature.

3.2.6. Irreversible strain

A Maxwell dash-pot component is used to describe the permanent deformation:

$$\boldsymbol{\sigma} = \gamma_{\mathrm{ir}}\dot{\boldsymbol{\varepsilon}}_{\mathrm{ir}} \tag{21}$$

Based on the experimental observation (Tobushi et al., 1997), $\boldsymbol{\gamma}_{\mathrm{ir}}$ can be assumed as a function of temperature in the vicinity of θ_{g} but almost constant outside the phase transition region. The temperature dependence of $\boldsymbol{\gamma}_{\mathrm{ir}}$ can be considered in the manner of William-Landel-Ferry (WLF) equation:

$$\gamma_{\mathrm{ir}}(\theta) = \gamma_{\mathrm{ir}}^{0} \exp\left(\frac{-c_1(\theta - \theta_r)}{c_2 + \theta - \theta_r}\right) \tag{22}$$

where c_1, c_2, γ_{ir}^{o}, and θ_r are constants.

3.3. Summary of the model

As discussed in the previous section, the complicated thermomechanical behavior of the SMP based self-healing syntactic foam is studied with a comprehensive model, which separately considers the material behavior in the manner of multi-phase and different mechanisms. The important features of this model are summarized in Table 1.

4. Thermodynamic consideration

In order to prove the thermodynamic consistency as well as to give a better understanding of this material model, the thermodynamic framework of the constitutive modeling is discussed in this section.

As a result of the physical understanding of the deformation mechanisms and experimental results (Liu et al., 2006; Helm and Haupt, 2003; Holzapfel, 2000) in combination with specific consideration in our case, the Helmholtz free energy function is expressed in the form:

$$\psi = \psi_{m\theta}\left(\theta, \boldsymbol{\varepsilon}_{\mathrm{g}}, \boldsymbol{\varepsilon}_{\mathrm{a}}, \boldsymbol{\varepsilon}_{\mathrm{a}}^{\mathrm{v}}, \boldsymbol{\varepsilon}_{\mathrm{f}}, \boldsymbol{\varepsilon}_{\mathrm{f}}^{\mathrm{neq}}, \phi\right) + \psi_s(\theta, \boldsymbol{\varepsilon}_s), \tag{23}$$

where $\psi_{m\theta}$ consists of the mechanical energy, the thermal energy and the initial free energy of the material; ψ_s represents the free energy due to the entropic strain storage.

Then the second Law of thermodynamics applies in the form of the Clausius-Duhem inequality (Holzapfel, 2000):

$$\boldsymbol{\sigma} : \boldsymbol{\varepsilon} - \rho(\dot{\psi} + \eta\dot{\theta}) - \boldsymbol{q} \cdot \frac{\nabla\theta}{\theta} \geqslant 0, \tag{24}$$

where η represents the entropy, $\boldsymbol{q}$ denotes the heat flux, and ρ is the density.

Table 1
Summary of the model.

Total strain	$\boldsymbol{\varepsilon} = (1 - f_{\mathrm{p}})\boldsymbol{\varepsilon}_{\mathrm{g}} + f_{\mathrm{p}}(1 - \phi)\boldsymbol{\varepsilon}_{\mathrm{a}} + f_{\mathrm{p}}\phi\boldsymbol{\varepsilon}_{\mathrm{f}} + f_{\mathrm{p}}\boldsymbol{\varepsilon}_{\mathrm{s}} + \boldsymbol{\varepsilon}_{\theta} + \boldsymbol{\varepsilon}_{\mathrm{ir}}$
Frozen phase volume fraction evolution	$\phi = 1 - \frac{1}{1+\exp(-(\theta-\theta_g)/A)}$
Mechanisms	
Glass balloons (g)	$\boldsymbol{\varepsilon}_{\mathrm{g}} = \mathbf{S}_{\mathrm{g}}\boldsymbol{\sigma}$
Active phase (a)	$\boldsymbol{\varepsilon}_{\mathrm{a}} = \boldsymbol{\varepsilon}_{\mathrm{a}}^{\mathrm{e}} + \boldsymbol{\varepsilon}_{\mathrm{a}}^{\mathrm{v}} \quad \boldsymbol{\sigma} = \mathbf{C}_{\mathrm{a}}^{\mathrm{r}}\boldsymbol{\varepsilon}_{\mathrm{a}}^{\mathrm{v}} + \gamma_{\mathrm{a}}\dot{\boldsymbol{\varepsilon}}_{\mathrm{a}}^{\mathrm{v}}$
Frozen phase (f)	$\boldsymbol{\sigma} = \mathbf{C}_{\mathrm{f}}^{\mathrm{r}}\boldsymbol{\varepsilon}_{\boldsymbol{f}} + \boldsymbol{\sigma}_{\mathbf{f}}^{\mathrm{neq}} \quad \dot{\boldsymbol{\varepsilon}}_{\mathbf{f}}^{\mathrm{eq}} = (\mathbf{S}_{\mathbf{f}}^{e}\dot{\boldsymbol{\sigma}}_{\mathbf{f}}^{\mathrm{neq}} + \gamma_f^{-1}\boldsymbol{\sigma}_f^{\mathrm{neq}})$
Entropic storage (s)	$\boldsymbol{\varepsilon}\mathrm{s} = \int_{t_0}^{t} \boldsymbol{\varepsilon}_{\alpha}(\tau)\phi'(\tau)d\tau$
Thermal (θ)	$\boldsymbol{\epsilon}_{\theta} = \int_{\theta_0}^{\theta} \alpha\mathbf{I}\, d\theta$
Irreversible (ir)	$\boldsymbol{\sigma} = \gamma_{\mathrm{ir}}\dot{\boldsymbol{\epsilon}}_{\mathrm{ir}} \quad \gamma_{\mathrm{ir}} = \gamma_{\mathrm{ir}}^{0}\exp\left(\frac{-c_1(\theta-\theta_r)}{c_2+\theta-\theta_r}\right)$

In most cases, the inequality is expediently divided into the thermal dissipation inequality:

$$-\boldsymbol{q}\cdot\frac{\nabla\theta}{\theta}\geqslant 0, \tag{25}$$

and the internal dissipation inequality:

$$\boldsymbol{\sigma}:\boldsymbol{\varepsilon}-\rho(\dot{\psi}+\eta\dot{\theta})\geqslant 0, \tag{26}$$

The validity of the thermal dissipation inequality (Eq. (25)) is guaranteed in the Fourier-model, where $\boldsymbol{q} = -\lambda\Delta\theta$ with $\lambda > 0$.

Then we introduce the free energy (Eq. (23)) into the internal dissipation inequality (Eq. (26)) in combination with the Cauchy strain decomposition (Eq. (12)), it leads to:

$$\begin{aligned}\left((1-f_p)\boldsymbol{\sigma}-\rho\frac{\partial\psi_{m\theta}}{\partial\boldsymbol{\varepsilon}_g}\right):\dot{\boldsymbol{\varepsilon}}_g&+\left(f_p(1-\phi)\boldsymbol{\sigma}-\rho\frac{\partial\psi_{m\theta}}{\partial\boldsymbol{\varepsilon}_a}\right):\dot{\boldsymbol{\varepsilon}}_a\\&+\left(f_p\phi\boldsymbol{\sigma}-\rho\frac{\partial\psi_{m\theta}}{\partial\boldsymbol{\varepsilon}_f}\right):\dot{\boldsymbol{\varepsilon}}_f\\&-\rho\frac{\partial\psi_{m\theta}}{\partial\boldsymbol{\varepsilon}_a^v}-\rho\frac{\partial\psi_{m\theta}}{\partial\boldsymbol{\varepsilon}_f^{neq}}\dot{\boldsymbol{\varepsilon}}_f^{neq}+\boldsymbol{\sigma}:\dot{\boldsymbol{\varepsilon}}_{ir}\\&+\left(f_p\boldsymbol{\sigma}-\rho\frac{\partial\psi_s}{\partial\boldsymbol{\varepsilon}_s}\right):\dot{\boldsymbol{\varepsilon}}_s+\boldsymbol{\sigma}:\Delta\dot{\boldsymbol{\varepsilon}}_m\\&-\rho\frac{\partial\psi_{m\theta}}{\partial\Phi}\dot{\phi}-\rho\left(\frac{\partial\psi}{\partial\theta}+\eta\right)\dot{\theta}\geqslant 0,\end{aligned} \tag{27}$$

where $\Delta\boldsymbol{\varepsilon}_m = f_p\int_0^{\phi}(\boldsymbol{\varepsilon}_f-\boldsymbol{\varepsilon}_a)d\phi$, then $\Delta\dot{\boldsymbol{\varepsilon}}_m = f_p(\boldsymbol{\varepsilon}_f-\boldsymbol{\varepsilon}_a)\dot{\phi}$.

Following standard arguments, the following potential relation for the stress tensor and the entropy is suggested to guarantee the inequality:

$$\eta = -\frac{\partial\psi}{\partial\theta}+\frac{1}{2}\boldsymbol{\sigma}:(\dot{\boldsymbol{\varepsilon}}_\theta+\Delta\dot{\varepsilon}_m). \tag{28}$$

If we further introduce the following elastic part of the free energy function:

$$\begin{aligned}\psi_{m\theta} = \frac{1}{\rho}\Bigg\{&(1-f_p)\left(\frac{1}{2}\mathbf{C}_g:\boldsymbol{\varepsilon}_g:\boldsymbol{\varepsilon}_g\right)+f_p(1-\phi)\left(\frac{1}{2}\mathbf{C}_a^e:(\boldsymbol{\varepsilon}_a-\boldsymbol{\varepsilon}_a^v)\right)\\&:\left(\boldsymbol{\varepsilon}_a-\boldsymbol{\varepsilon}_a^v\right)+f_p\phi\left(\frac{1}{2}(\boldsymbol{\varepsilon}_f-\boldsymbol{\varepsilon}_f^{neq})+\frac{1}{2}\mathbf{C}_f^r:\boldsymbol{\varepsilon}_f:\boldsymbol{\varepsilon}_f\right)\Bigg\}\\&+c_{d0}\left\{(\theta-\theta_0)-\theta\log\frac{\theta}{\theta_0}\right\}+\{\psi_{a0}+\phi\Delta_0\}\end{aligned} \tag{29}$$

where the second bracketed term describes the pure thermal contribution, and c_{d0} denotes the specific heat capacity (Liu et al., 2006); the third bracketed term represents the initial free energy of the material. ψ_{a0} denotes the initial free energy of the active phase and $\Delta\psi = \Delta\kappa_0 - \theta\Delta\eta_0$, where $\Delta\kappa_0 = \kappa_0^f - \kappa_0^a$ and $\Delta\eta_0 = \eta_0^f - \eta_0^a$. κ_0 and η_0 represent the initial internal energy and entropy (Helm and Haupt, 2003).

Then, based on the previous stress analysis of each phase, the internal dissipation inequality (Eq. (27)) reduces to:

$$\begin{aligned}&\gamma_a:\dot{\boldsymbol{\varepsilon}}_a^v:\dot{\boldsymbol{\varepsilon}}_a^v+\gamma_f:\dot{\boldsymbol{\varepsilon}}_f^{neq}:\dot{\boldsymbol{\varepsilon}}_f^{neq}+\gamma_{ir}:\dot{\boldsymbol{\varepsilon}}_{ir}\\&:\dot{\boldsymbol{\varepsilon}}_{ir}-\rho\Delta\psi\dot{\phi}+\left(f_p\boldsymbol{\sigma}-\rho\frac{\partial\psi_s}{\partial\boldsymbol{\varepsilon}_s}\right):\dot{\boldsymbol{\varepsilon}}_s\geqslant 0\end{aligned} \tag{30}$$

The first three terms in the residual dissipation inequality (Eq. (30)) represent the rate of energy necessary to overcome internal dissipative resistance. Therein, γ is the viscosity tensor, so they must be positive definite. Consequently, these three terms are always non-negative. Furthermore, Helm and Haupt (2003) proposed an evolution equation for the temperature-induced phase transition in the shape memory alloy constitutive model, $\dot{\phi} = -\frac{|\dot{\phi}|}{\Delta\theta}\frac{\Delta\psi}{|\Delta\psi|}$, if such assumption also stands in the current issue of SMP, where $\Delta\theta$ represents the phase transition temperature range, it yields that the fourth term is also non-negative. Then the proportional relation $\dot{\boldsymbol{\varepsilon}}_s \sim \left(f_p\boldsymbol{\sigma}\frac{\partial\psi_s}{\partial\boldsymbol{\varepsilon}_s}\right)^D$ (Helm and Haupt, 2003) guarantees the positiveness of the fifth term, where $(f_p\boldsymbol{\sigma}-\rho\frac{\partial\psi_s}{\partial\boldsymbol{\varepsilon}_s})$ is the deviatoric stress tensor. As a result, the Clausius-Duhem inequality is satisfied and the proposed constitutive model is thermodynamically admissible for an arbitrary thermomechanical process.

5. Model validation

The constitutive model was computed in MATLAB. The simulations are compared with the experimental results presented in the literature. The details of the stress-controlled programming, confined shape recovery, and free recovery can be found in (Li and Nettles, 2009). The material parameters are listed in Table 2.

5.1. Stress-controlled programming and free recovery

During the experiment, a SMP based syntactic foam sample was stressed by a constant load $\boldsymbol{\sigma}_0$ at θ_H and then held for a time period t_1 (Step 1). After that the sample was naturally cooled down to θ_L with the same constant load (Step 2). The cooling rate can be determined by Newton's Law of Cooling: $\frac{d\theta}{dt} = k(\theta-\theta_s)$. θ_s is the surrounding environment temperature. Once the temperature reaches θ_L, the load was removed (Step 3) and the sample was then heated up to θ_H without any loading (free recovery) (Step 4).

In order to fully understand the whole thermomechanical cycle, the numerical simulation is conducted in the time scale (Fig. 8(a)). The model shows the general behavior of the compressive strain in the thermomechanical history which increases rapidly at θ_H (Step 1) and reaches the plateau during cooling and unloading (Steps 2 and 3) then decreases as temperature rises (Step 4). In general, the model is in agreement with the test results.

5.2. Constrained stress recovery

After the stress-controlled programming (the first three steps in Fig. 8(a)), the fully constrained recovery process is carried out with boundary conditions of fixed-strain constraint (zero initial stress) and a constant heating rate, aiming to characterize the stress recovery feature of the SMP based syntactic foam. Fig. 8(b) shows the stress *vs.* temperature behavior from the experiment and the numerical simulation. The two curves agree fairly well especially after the peak stress. The difference between the model and the experiment in the initial part probably comes from the lack of close contact between the specimen and the load cell at the beginning of the loading.

6. Prediction and discussion

6.1. Dependence on microballoon volume fraction

Superior to pure shape memory polymer, the thermomechanical properties of the studied SMP based syntactic foam can be modified without complex chemical procedures. Fig. 9 shows the predicted thermomechanical behavior of two SMP based syntactic foams with different volume fractions of microballoon inclusions. It appears that more glass microballoons addition leads to a stiffer material and a higher peak recovery stress, but does not affect the recoverability. Thus, with proper adjustment of the percentage of the compositions, one can customize the foam to satisfy both the conventional mechanical capability demands and the material intelligence requirements.

Table 2
Material parameters of the preliminary thermoviscoelastic constitutive model.

Model components	Material parameters	Values
Volume fraction of matrix	f_p	0.6
Frozen fraction evolution (ϕ)	A; θ_g (°C)	1.5; 71
Glass microballoon	E_g (MPa)	7E4
Active phase	E_a^e (MPa)	9.38
	E_a^v (MPa)	1.90
	γ_a (MPa s)	332
Frozen phase	E_f^{eq} (MPa)	15
	E_f^{neq} (MPa)	247
	γ_f (MPa s)	2E9
Thermal expansion coefficient	$\alpha(\theta)$ (°C^{-1})	1.72E−4−1.40E−6 $\cdot\theta$
Irreversible strain	γ_{ir} (MPa s) ($\theta \geqslant \theta_H$); θ_H (°C)	1.2E5; 79
	γ_{ir} (MPa s) ($\theta \leqslant \theta_i$); θ_i (°C)[1]	7E8; 55
	γ_{ir}^0(MPa s);	1.2E5
	c_1; c_2(°C); θ_r (°C)	3.06; 34.07; 79
Experimental setup	θ_L (°C); t_1 (min); $\boldsymbol{\sigma}_0$ (MPa)	22; 30; 0.263
Cooling rate	k (s^{-1}); θ_S	4.6E−5; 20
Heating rate	h_v (°C/min)	0.3

[1] θ_i represents the temperature at which the phase transition starts during heating.

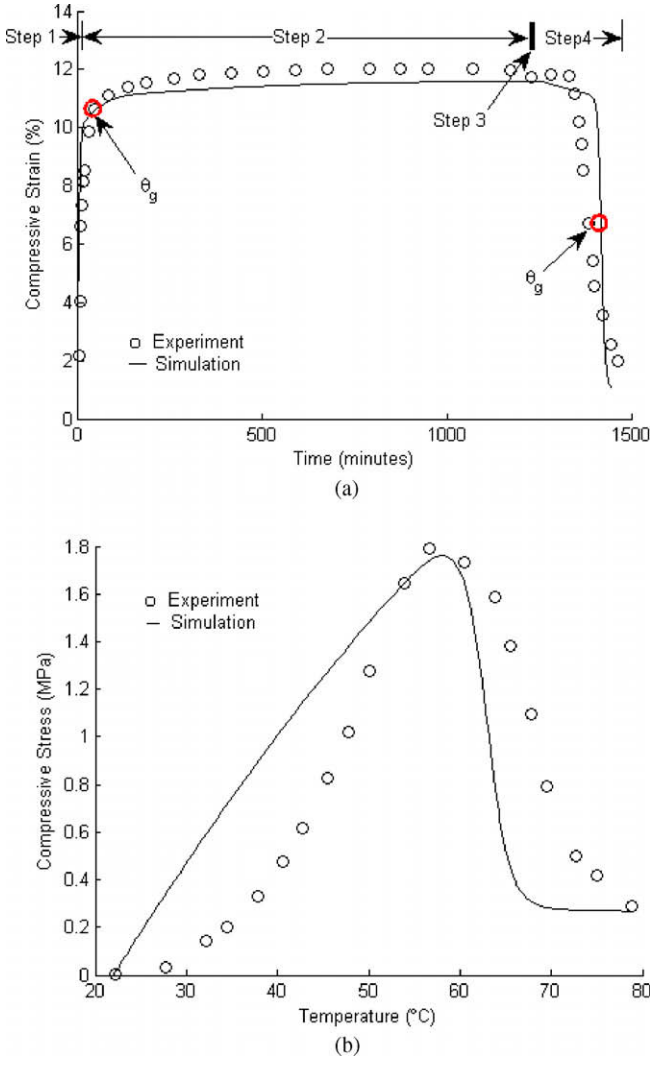

Fig. 8. Numerical simulations of thermo-mechanical behavior of the SMP based syntactic foam (a) stress-controlled strain fixity and free recovery (b) constrained stress recovery.

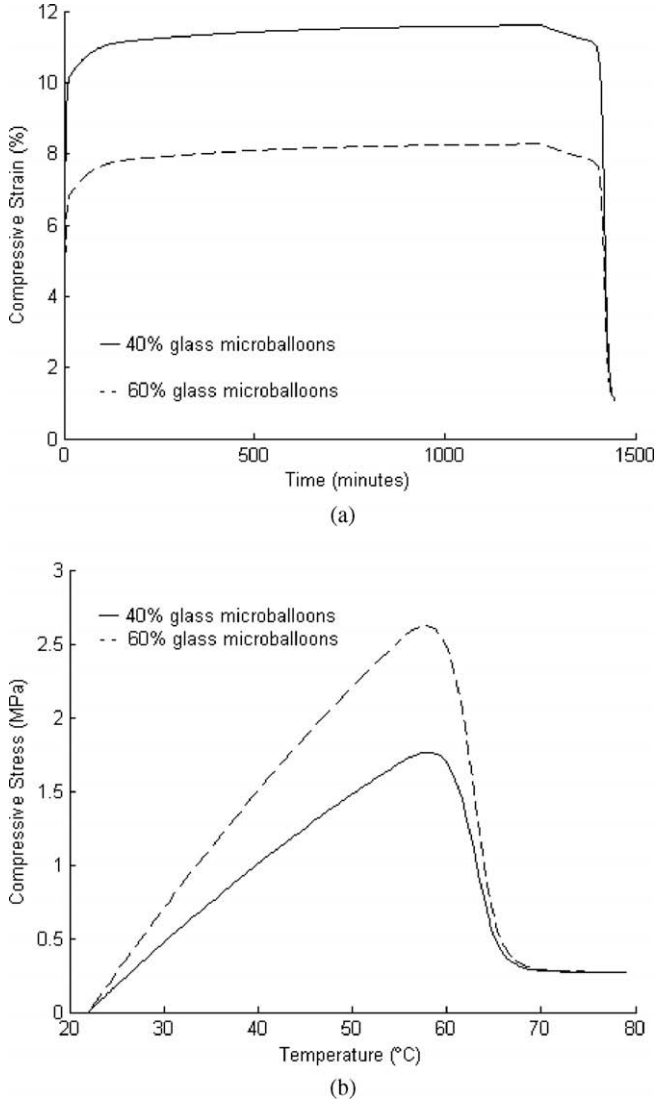

Fig. 9. Effect of microballoon volume on the (a) strain history throughout the thermomechanical cycle and (b) stress evolution during shape recovery.

6.2. Dependence on microballoon stiffness

Another approach to tailor the mechanical properties of the SMP based syntactic foam is to modify the particle stiffness. Generally, the hallow particles have different stiffness with different wall thickness. If we assume that the properties of the ITZ are only dependent on the geometry and the surface composition of the hallow particles, the syntactic foams with different particle wall thickness but the same particle size will have the same equivalent polymer matrix. The addition of soft inclusions (with thinner wall) consequently reduces the foam stiffness and yields a slightly higher strain level during step 1 and step 2 (loading and cooling) as shown in Fig. 10(a). But because the additional elastic strain originates from the stiffness reduction of the hallow particles, a larger strain spring-back occurs immediately after the load is removed (Step 3 in Fig. 10(a)). The most significant change appears in the constrained stress recovery (Fig. 10(b)) as the peak recovery stress is clearly increased with stiffer particles. Again, the recoverability of the foam is not affected by the change of the stiffness of the glass microballoons.

6.3. Dependence on cooling and heating rate

The structural relaxation suggests a temperature rate dependence of the SMP based syntactic foam. Fig. 11(a) shows the effect

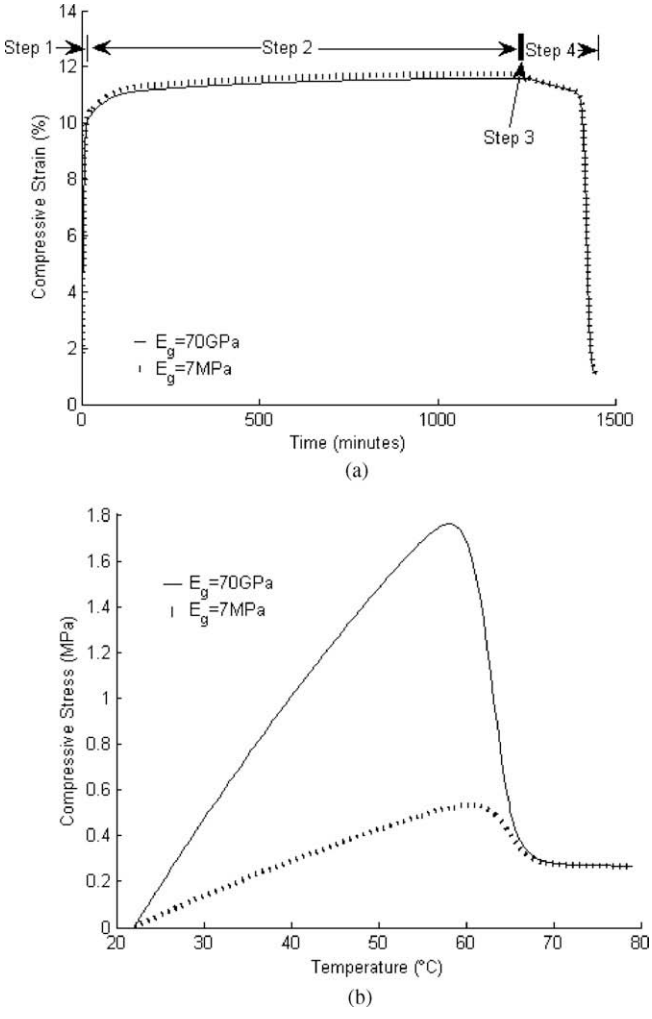

Fig. 10. Effect of microballoon stiffness on the (a) strain history throughout the thermomechanical cycle and (b) stress evolution during shape recovery.

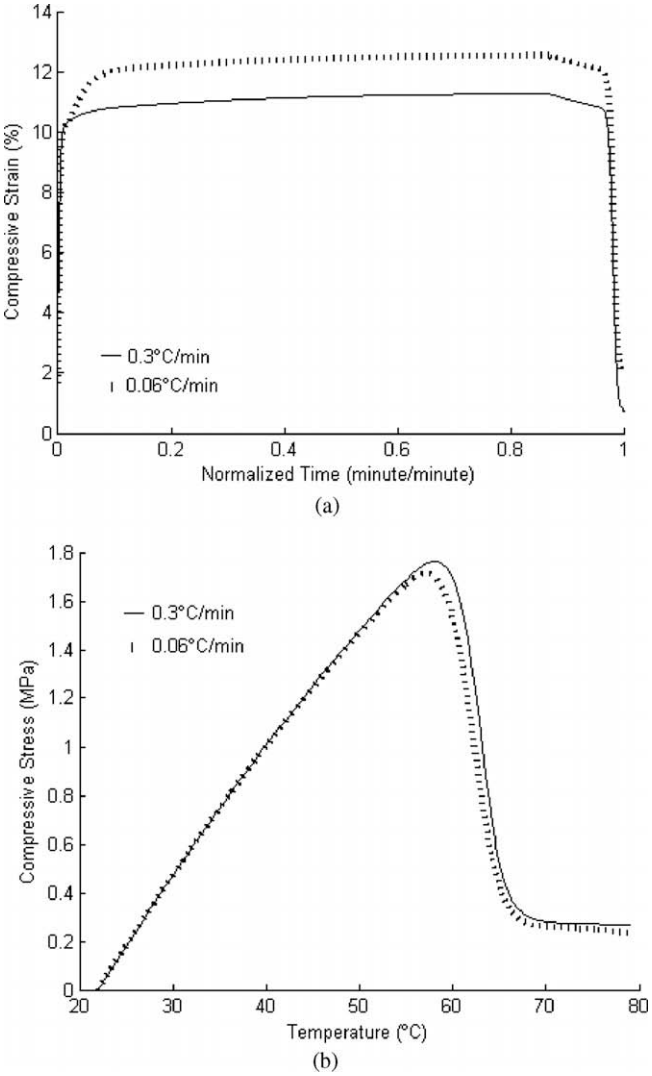

Fig. 11. Effect of temperature rate on the (a) strain history throughout the thermomechanical cycle and (b) stress evolution during shape recovery.

of cooling rate on the strain in the thermomechanical cycle by maintaining the same heating rate in terms of the normalized time (t/t_0) (t_0 is the total time period for the programming and re-heating process) and Fig. 11(b) shows the effect of heating rate on the recovered compressive stress during the constrained shape recovery step (Step 4 in the thermomechanical cycle) in terms of the normalized time (t/t_0). It can be concluded from the illustrations that fast cooling reduces the irreversible strain and a higher heating rate leads to a slightly higher peak stress and slightly higher recovered stress.

6.4. Constrained strain recovery

As mentioned earlier, in practice, the syntactic foam is typically used as a core material and incorporated into the sandwich composite structure where two stiff skins are attached to its top and bottom surfaces (Fig. 12(a)). Therefore strictly speaking, during a free recovery process of a sandwich structure, the SMP based syntactic foam core is actually experiencing a partially confined process with a constant stress constraint. Such constant stress can be expressed as $\sigma = W/S$, where W denotes the skin weight and external confinement load and S is the foam surface area. Fig. 12(b) shows the recovery strain response of the SMP based

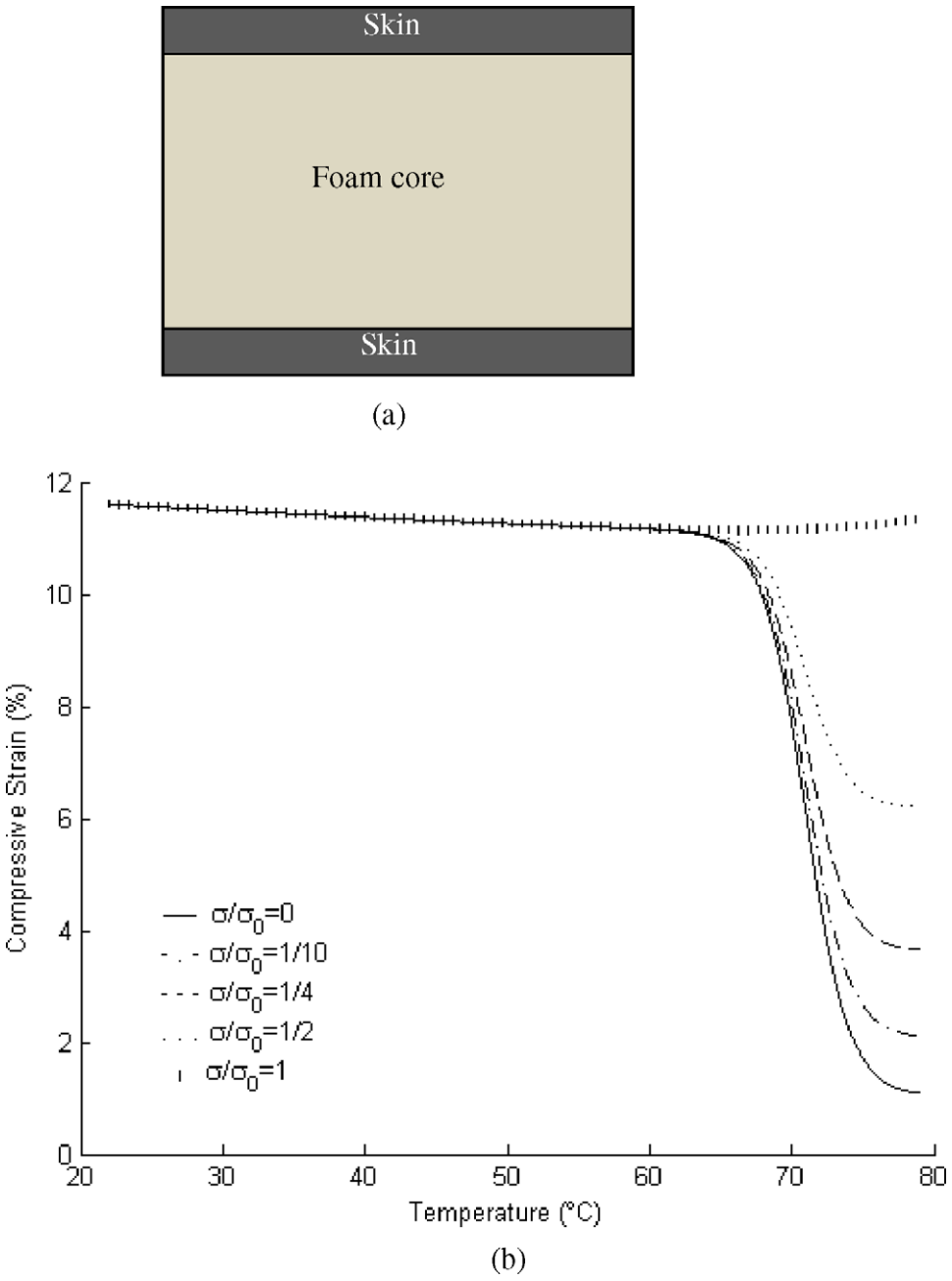

Fig. 12. (a) Illustration of a SMP based syntactic foam cored sandwich composite structure (b) the recovery strain response of the sandwich structures to different external stresses.

syntactic foam core for various constraint stress levels. If the same foam core is considered in these cases, the results indicate that heavier skins or higher external confinement load resist the recovery of the shape externally (small strain recovered externally). Because the recoverability of the foam is not affected by the confinement load, the reduced external strain translates to an increases in internal deformation, i.e., the material will be pushed into the internal open space such as cracks, leading to self-sealing of the damaged foam.

7. Conclusions

A thermomechanical constitutive model was developed for an innovative SMP based syntactic foam. With the effects of classical viscoelasticity and pseudo-plasticity incorporated, the model reasonably captures the essential elements of the shape memory or self-healing response. The model was proved through the Clausiu-Duhem inequality for thermodynamic consistency and verified against the uniaxial experimental results. A parametric study was further conducted to feature the future design and optimization of such intelligent foam material. The main results of the simulation are:

(1) The thermomechanical properties of the SMP based syntactic foam material could be customized by adjusting the volume fraction and the stiffness of the hallow particles. High particle volume fraction or stiffer inclusions strengthened the material and increased the recovery peak stress. An optimal material could be achieved through the adjustment of these two factors.

(2) Fast cooling reduced the permanent deformation thus enhanced the recoverability, while fast re-heating increased the peak stress and recovery stress because of the reduction in irreversible structure relaxation.
(3) External confinement during shape recovery significantly affects the recovery stress or strain. As the external confinement stress increases, the externally recovered strain reduces but the internal deformation increases, leading to better self-sealing of the internal damage such as crack.
(4) More realistic models such as mesomechanical model to avoid homogeneous stress assumption, consideration of nonlinear behavior below T_g, etc., will be developed in future studies to reduce the discrepancies between the experimental and theoretical results.

Acknowledgements

The work is funded by NASA/EPSCoR under Grant number NASA/LEQSF(2007-10)-Phase3-01 and NSF under Grant number CMMI 0900064. The authors gratefully thank Mr. Damon Nettles, Mr. Hari Konka, Dr. Kun Lian for the assistance in the DMA test, Mr. Zhaoyuan Liu, Dr. Donghui Zhang, and Dr. Haoyu Tang for the discussion about the FTIR test results, and Dr. Dongmei Cao for the help in acquiring the SEM images.

References

Anderson, T.F., Walters, H.A., Glesner, C.W., 1970. Castable, sprayable, low density foam and composites for furniture, marble, marine. J. Cell. Plast. 6, 171–178.
Andreozzi, L., Faetti, M., Zulli, F., Giordano, M., 2004. Enthalpy relaxation of polymers: comparing the predictive power of two configurational entropy models extending the AGV approach. Eur. Phys. J.B 41, 383–393.
Berriot, J., Montes, H., Lequiux, F., Long, D., Sotta, P., 2003. Gradient of glass transition temperature in filled elastomers. Eur. Lett. 64 (1), 50–56.
Bhattacharyya, A., Tobushi, H., 2000. Analysis of the isothermal mechanical response of a shape memory polymer rheological model. Polym. Eng. Sci. 2000, 2498–2510.
Blaiszik, B.J., Sottos, N.R., White, S.R., 2008. Nanocapsules for self-healing materials. Comp. Sci. Technol. 68, 978–986.
Boyce, M.C., Arruda, E.M., 1993. Three-dimensional constitutive model for the large stretch behavior of rubber elastic materials. J. Mech. Phys. Solids 41 (2), 389–412.
Chen, Y.H., Lagoudas, D.C., 2008a. A constitutive theory for shape memory polymers. Part II-A linearized model for small deformations. J. Mech. Phys. Solids 56, 1766–1778.
Chen, Y.H., Lagoudas, D.C., 2008b. A constitutive theory for shape memory polymers. Part I-large deformations. J. Mech. Phys. Solids 56, 1752–1765.
Diani, J., Gall, K., 2007. Molecular dynamics simulations of the shape-memory behaviour of polyisoprene. Smart Mater. Struct. 16, 1575–1583.
El-Hadek, M.A., Tippur, H.V., 2003. Dynamic fracture parameters and constraint effects in functionally graded syntactic epoxy foams. Int. J. Solids Struct. 40, 1885–1906.
Gall, K., Yakacki, C.M., Liu, Y., Shandas, R., Willett, N., Anseth, K.S., 2005. Thermomechanics of the shape memory effect in polymers for biomedical applications. J. Biomed. Mater. Res. A 73, 339–348.
Gupta, N., 2007. A functionally graded syntactic foam material for high energy absorption under compression. Mater. Lett. 61, 979–982.
Helm, D., Haupt, P., 2003. Shape memory behavior: modeling within continuum thermomechanics. Int. J. Solids Struct. 40, 827–849.
Holzapfel, G.A., 2000. Nonlinear Solid Mechanics. John Wiley & Sons, Ltd., New York.
Kafka, V., 2001. Mesomechanical Constitutive Modeling. World Scientific, Singapore.
Kafka, V., 2008. Shape memory polymers: a mesoscale model of the internal mechanism leading to the SM phenomena. Int. J. Plast. 24, 1533–1548.
Khan, A.S., Lopez-Pamies, O., Rehan, K.R., 2006. Thermo-mechanical large deformation response and constitutive modeling of viscoelastic polymers over a wide range of strain rates and temperatures. Int. J. Plast. 22, 581–601.
Kontou, E., 2005. Viscoplastic deformation of an epoxy resin at elevated temperatures. J. Appl. Polym. Sci. 101 (3), 2027–2033.
Kröner, E., 1960. Allgemeine kontinuumstheorie der versetzungen Arch. Rat. Mech. Anal., 273–334.
Lee, E.H., 1969. Elastic-plastic deformation at finite strains. ASME J. Appl. Mech. 36, 1–6.
Li, G., Chakka, V.S., 2010. Isogrid stiffened syntactic foam cored sandwich structure under low velocity impact. Compos. Appl. Sci. Manuf. 41 (1), 177–184.
Li, G., John, M., 2008. A self-healing smart syntactic foam under multiple impacts. Comp. Sci. Technol. 68 (15–16), 3337–3343.
Li, G., Muthyala, V.D., 2008. Impact characterization of sandwich structures with an intergrated orthogrid stiffened syntactic foam core. Comp. Sci. Technol. 68 (9), 2078–2084.
Li, G., Nettles, D., 2009. Thermomechanical characterization of a shape memory polymer based self-repairing syntactic foam. Polymer, (Available on-line December 22, 2009) doi:10.1016/j.polymer.2009.12.002.
Li, G., Nji, J., 2007. Development of rubberized syntactic foam. Compos. Appl. Sci. Manuf. 38 (6), 1483–1492.
Lion, A., 1997. On the large deformation behavior of reinforced rubber at different temperatures. J. Mech. Phys. Solids 45, 1805–1834.
Liu, Y., Gall, K., Dunn, ML., McCluskey, P., 2004. Thermomechanics of shape memory polymer nanocomposites. Mech. Mater. 36, 929–940.
Liu, Y., Gall, K., Dunn, M.L., Greenberg, A.R., Diani, J., 2006. Thermomechanics of shape memory polymers: uniaxial experiments and constitutive modeling. Int. J. Plast. 22, 279–313.
Liu, Y.L., Chen, Y.W., 2007. Thermally reversible cross-linked polyamides with high toughness and self-repairing ability from maleimideand furan-functionalized aromatic polyamides. Macro. Chem. Phys. 208, 224–232.
Lu, S.C.H., Pister, K.S., 1975. Decomposition of deformation and representation of the free energy function for isotropic thermoelastic solids. Int. J. Solids Struct. 11, 927–934.
Morshedian, J., Khonakdar, H.A., Rasouli, S., 2005. Modeling of shape memory induction and recovery in heatshrinkable polymers. Macromol. Theory Simulat. 14, 428–434.
Nguyen, T.D., Qi, H.J., Castro, F., Long, K.N., 2008. A thermoviscoelastic model for amorphous shape memory polymers: incorporating structural and stress relaxation. J. Mech. Phys. Solids 56, 2792–2814.
Nji, J., Li, G., 2008. A CaO enhanced rubberized syntactic foam. Compos. Appl. Sci. Manuf. 39 (9), 1404–1411.
Qi, H.J., Nguyen, T.D., Castro, F., Yakacki, C.M., Shandas, R., 2008. Finite deformation thermo-mechanical behavior of thermally induced shape memory polymers. J. Mech. Phys. Solids 56, 1730–1751.
Pang, J.W.C., Bond, I.P., 2005. A hollow fibre reinforced polymer composite encompassing self-healing and enhanced damage visibility. Comp. Sci. Technol. 65, 1791–1799.
Rizzi, E., Papa, E., Corigliano, A., 2000. Mechanical behavior of a syntactic foam: experiments and modeling. Int. J. Solids Struct. 37, 5773–5794.
Song, B., Chen, W., Frew, D.J., 2004. Dynamic compressive response and failure behavior of an epoxy syntactic foam. J. Comp. Mater. 38, 915–936.
Sperling, L.H., 2006. Introduction to Physical Polymer Science. John Wiley& Sons, Inc., New Jersey.
Tobushi, H., Hara, H., Yamada, E., Hayashi, S., 1996. Thermomechanical properties in a thin film of shape memory polymer of polyurethane series. Smart Mater. Struct. 5, 483–491.
Tobushi, H., Hashimoto, T., Hayashi, S., Yamada, E., 1997. Thermomechanical constitutive modeling in shape memory polymer of polyurethane series. J. Intell. Mater. Syst. Struct. 8, 711–718.
Tobushi, H., Hashimoto, T., Ito, N., Hayashi, S., Yamada, E., 1998. Shape fixity and shape recovery in a film of shape memory polymer of polyurethane series. J. Intell. Mater. Sys. Struct. 9, 127–136.
Toohey, K.S., Sottos, N.R., Lewis, J.A., Moore, J.S., White, S.R., 2007. Self-healing materials with microvascular networks. Nat. Mater. 6, 581–586.
Tüdős, F., David, P.K., 1996. Comments on the interpretation of temperature dependence of processes in polymers. J. Therm. Anal. Cal. 47 (2), 589–593.
Varley, R.J., van der Zwaag, S., 2008. Towards an understanding of thermally activated self-healing of an ionomer system during ballistic penetration. Acta Mater. 56, 5737–5750.
Vishay Micro Measurement, 2007. Measurement of thermal expansion coefficient using strain gages. Tech Note, TN-513-1.
Yakacki, C.M., Shandas, R., Lanning, C., Rech, B., Eckstein, A., Gall, K., 2007. Unconstrained recovery characterization of shape-memory polymer networks for cardiovascular applications. Biomaterials 28, 2255–2263.
Zako, M., Takano, N., 1999. Intelligent material systems using epoxy particles to repair microcracks and delamination damage in GFRP. J. Intell. Mater. Syst. Struct. 10, 836–841.